Wireless Power Transfer

ARTICLE

Open Access

https://doi.org/10.48130/wpt-0025-0009

Wireless Power Transfer **2025**, 12: e013

WPT system for constant current and constant voltage charging based on switched resonant frequency

Zhen Guo, Zhaodong Li*, Haitao Yu, Hailong Zhang, Jiqiu Nai, Shuang Chen, Ranran Liu and Min Zhang

College of Information and Control Engineering, Qingdao University of Technology, Qingdao 266520, China

* Corresponding author, E-mail: 18335996206@163.com

Abstract

This paper designs and implements an innovative WPT system that possesses the capability to seamlessly switch between constant current (CC) and constant voltage (CV) outputs, thereby fully satisfying the various charging requirements of batteries for both CC and CV. An S/S compensated WPT system is proposed that enables battery charging in both CC and CV by switching between two specific frequencies. In addition, load estimation and output current estimation are employed to estimate the output voltage. The output voltage will be used as a criterion for the conversion of the operating frequency of the CC to the operating frequency of the CV. The system is simple and does not require complex control strategies, primary and secondary side communication, or additional devices to reconfigure the circuit topology. The charging output of the proposed system can reach 0.38 A/23 V based on an S/S topology. Both through theoretical analysis and computer simulations, the feasibility of the proposed WPT system has been verified. The experimental results show that a CC output of 0.38 A and a CV output of 23 V can be realized by switching the resonant frequency at a constant input voltage.

Citation: Guo Z, Li Z, Yu H, Zhang H, Nai J, et al. 2025. WPT system for constant current and constant voltage charging based on switched resonant frequency. *Wireless Power Transfer* 12: e013 https://doi.org/10.48130/wpt-0025-0009

Introduction

Wireless power transfer (WPT) enables the transmission of power through electromagnetic coupling between terminal coils. Compared with the traditional wired charging method, the advantages of WPT technology include: safety, convenience, environmental adaptability, and mobility[1,2], and are extensively applied across multiple industrial domains, such as portable electronic equipment, LED lighting, medical, EVs, and underwater[3–7].

In practical applications, to extend battery life, the two-stage charging method combining constant current (CC), and constant voltage (CV) is commonly adopted. According to the charging profile provided[8], as illustrated in Fig. 1, the initial charging stage operates in constant current mode, where the charging current remains fixed while the charging voltage gradually increases. Once the charging voltage reaches a specified threshold, the system transitions to CV mode. During this phase, the charging voltage tends to stabilize. At the same time the charging current progressively diminishes until the charging process is concluded. It is worth noting that the equivalent load resistance of the battery varies during charging, introducing additional complexity into the design of the WPT system.

To realize CC and CV output of a WPT system under load variation, researchers have carried out numerous research in recent years. A closed-loop control system based on a DC-DC converter is proposed; however, the introduction of a DC-DC converter increases circuit costs, enhances system complexity, and adds additional losses[9]. A WPT system based on frequency control is presented, but the frequency splitting phenomenon caused by significant frequency changes undermined system stability[10]. A way of switching topologies by switching is proposed, but adds complexity to the circuit[11]. A WPT system that achieves CC and CV output is proposed[12,13], although it utilizes a larger number of compensation components. A multi-coil structure WPT system is presented; however, the mutual inductance between coils significantly affects system output[14,15]. A WPT system with an S/SP compensation structure is proposed; but it still necessitates communication between the primary and secondary sides, although requiring fewer compensation components[16]. A system for isolating a DC-DC converter by an LLC resonant circuit is presented, but it is complex and requires switching[17]. An LCL-S topology without communication is proposed, it increases the complexity of the system by using interference control and PI control on the primary and secondary sides[18]. A WPT system that does not require communication is proposed but still requires switching to reconfigure the circuit structure[19].

Considering the problems of the above WPT system, an S/S compensated WPT system is proposed that enables battery charging in both CC and CV by switching between two specific frequencies, which has a simple structure and uses fewer components to ensure the lightweight and high efficiency of the WPT system[20,21]. In addition, the system employs a method for load estimation and output current estimation and estimates the output voltage based on the estimated load and current. This output voltage will be used as a criterion for the conversion of the operating frequency of the CC to the operating frequency of the CV[22,23].

Theoretical analysis of the S/S compensation structure in WPT systems

System circuit model

The WPT system architecture with an S/S compensation structure is illustrated in Fig. 2. The system primarily comprises the following components: a DC input power supply U_d; a high-frequency inverter (consisting of four IGBT switches Q_1–Q_4 for converting DC to AC); transmitting coil inductance L_p and receiving coil inductance L_s; M represents the mutual inductance between the two coils; series capacitors C_p and C_s on the primary and secondary sides; R_1 and R_2 are the parasitic resistances of the primary and secondary sides, respectively; a rectifier circuit (composed of four MOSFET tubes D_1–D_4 for converting the received AC to DC for charging); an output

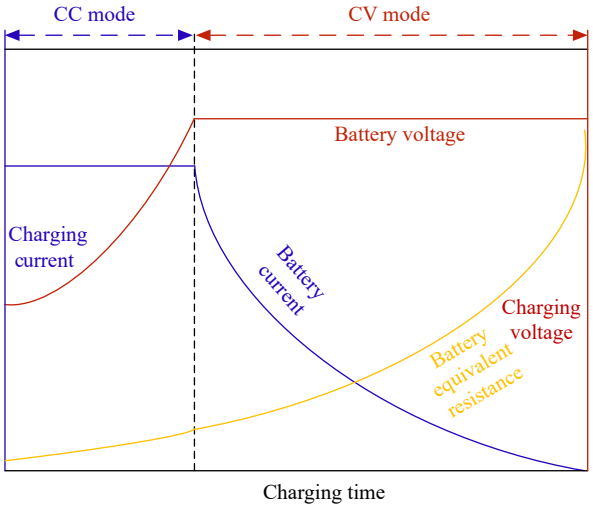

Fig. 1 Charging curve of a battery.

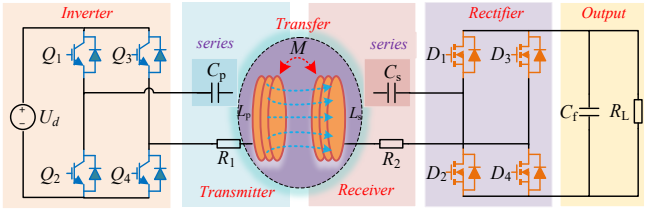

Fig. 2 WPT system architecture with S/S compensation structure.

filtering capacitor C_f; and R_L is the equivalent load resistance of the battery.

The voltage output of an inverter circuit is U_{in}, and the output current is represented by I_{in}. The current on the primary side is represented by I_p, while the current on the secondary side is represented by I_s. The AC equivalent resistance of the rectifier bridge and its subsequent components is represented by R_o, and the current flowing through this resistance is represented by I_o. The voltage across this resistance is represented by U_o. Figure 3 provides a detailed illustration of the equivalent circuit of a WPT system employing an S/S compensation strategy.

Based on the Fundamental Harmonic Approximation (FHA) method, the input voltage U_{in} can be mathematically represented as follows:

$$U_{in} = \frac{2\sqrt{2}}{\pi} U_d \cos\frac{\alpha}{2} \tag{1}$$

The rectifier bridge and its subsequent *AC* equivalent resistance R_o is:

$$R_o = \frac{2}{\pi} R_L \tag{2}$$

From the perspective of mutual inductance analysis, the WPT system featuring an S/S compensation structure can be regarded as equivalent to a mutual inductance model, as illustrated in Fig. 4.

Where Z_1 is the total impedance at the transmitting end, Z_2 is the total impedance at the receiving end, and the impedance at the receiving end is equivalent to the impedance at the transmitting end as Z_r.

$$\begin{cases} Z_1 = R_1 + \dfrac{1}{j\omega C_p} + j\omega L_p \\ Z_2 = R_o + R_2 + \dfrac{1}{j\omega C_s} + j\omega L_s \\ Zr = \dfrac{(\omega M)^2}{Z_2} \end{cases} \tag{3}$$

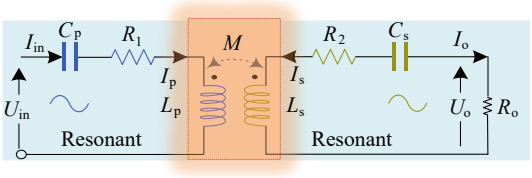

Fig. 3 Equivalent circuit diagram of the WPT system with S/S compensation structure.

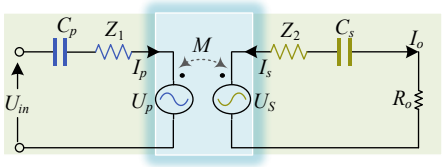

Fig. 4 Mutual inductance model of WPT system with S/S compensation structure.

CC characteristics

Using the mutual inductance model, the mutual inductance voltage U_s at the receiving end is:

$$U_s = j\omega M I_p = Z_2 I_s \tag{4}$$

Due to the effect of the receiving end, the voltage U_p reflected to the transmitting end is:

$$U_p = j\omega M I_s \tag{5}$$

Since the circuit operates in resonance, the total input impedance Z_{in} is:

$$Z_{in} = Z_1 + \frac{(\omega M)^2}{Z_2} = R_1 + \frac{(\omega M)^2}{R_o + R_2} \tag{6}$$

The voltage U_{in} the inverter output can also be expressed in the mutual inductance model as:

$$U_{in} = Z_1 I_p + j\omega M I_s = R_1 I_p + j\omega M I_s \tag{7}$$

Since the circuit is in full resonance, the output current amplitude I_s and current gain G_i are:

$$I_s = \left|\frac{U_{in} - R_1 I_p}{j\omega M}\right| = \frac{U_{in} - R_1 I_p}{\omega M} \tag{8}$$

$$G_i = \left|\frac{1}{j\omega M}\right| = \frac{1}{\omega M} \tag{9}$$

From Eqns (6), (8) and (9), the S/S topology achieves zero total input impedance Z_{in} at resonance, ensuring that the output current of the system remains load-independent, with a CC gain under varying load conditions.

CV characteristics

The current I_s at the receiving end passes through the load R_o, and in the resonant state:

$$I_s = \frac{U_s}{Z_2} = \frac{j\omega M I_p}{R_o + R_2} \tag{10}$$

Then the output voltage at the receiving end is:

$$U_o = I_s R_o = \frac{j\omega M I_p}{R_o + R_2} \cdot R_o \tag{11}$$

Since R_2 is much smaller than R_o, it will be $R_o + R_2 \approx R_o$ in Eqn (11), so the output voltage at the receiving end will be:

$$U_o = I_s R_o = \frac{j\omega M I_p}{R_o} \cdot R_o = j\omega M I_p \tag{12}$$

Associating Eqns (7) and (12), define the voltage gain as G_v:

$$Gv = \frac{U_o}{U_{in}} = \frac{j\omega M I_p}{R_1 I_p + j\omega M I_s} \quad (13)$$

From Eqns (12) and (13), the voltage outputted by the system is unaffected by the load, maintaining a consistent voltage gain across varying load conditions. Its total input impedance is the same as in CC mode, and there will be a small impedance angle because the S/S topology cannot achieve full resonance in CV mode.

Load estimation and output current estimation

For the WPT system with an S/S structure, a load estimation approach and an output current estimation approach are employed, and the output voltage is estimated based on the estimated load and output current, based on this output voltage, it is used as a criterion for frequency switching from CC to CV. The advantage is that it avoids real-time wireless communication on both sides.

According to Fig. 2, assuming the current flowing through the battery equivalent load R_L be $I_{L\_}$ in the case of considering only the voltage and current fundamental wave components, the current I_L is:

$$I_L = \frac{1}{\pi}\int_0^{\pi} I_S \sin(\omega t) d\omega t = \frac{2I_S}{\pi} \quad (14)$$

The power balance equation, neglecting the power losses in the rectifier during the following derivation is:

$$(I_L)^2 R_L = \left(\frac{I_S}{\sqrt{2}}\right)^2 R_o \quad (15)$$

In the equivalent circuit model shown in Fig. 3, based on Eqns (14) and (15), the current I_o flowing through R_o is derived as:

$$I_o = \frac{\pi}{2\sqrt{2}} I_L \quad (16)$$

Applying Kirchhoff's Voltage Law (KVL):

$$\begin{bmatrix} Z_1 & j\omega M \\ j\omega M & Z_2 \end{bmatrix} \begin{bmatrix} I_p \\ I_s \end{bmatrix} = \begin{bmatrix} U_{in} \\ 0 \end{bmatrix} \quad (17)$$

Based on Eqns (3) and (17), the resonant currents at the two coils can be deduced as:

$$\begin{cases} I_p = \dfrac{Z_2}{(\omega M)^2 + Z_1 Z_2} \times U_{in} \\ I_s = \dfrac{1}{j} \times \dfrac{(\omega M)}{(\omega M)^2 + Z_1 Z_2} \times U_{in} \end{cases} \quad (18)$$

Equation (18) demonstrates that changes in R_L affect I_p, subsequently altering the active power P_1 delivered to the battery, indicating a correlation between R_L and P_1. By calculating P_1, R_L can be indirectly estimated. The voltage-current on the battery equivalent load R_L can also be derived from the current I_p at the transmitting end through Eqns (2) and (18), it shows that even if we don't know R_L, the voltage-current on R_L can be regulated by I_p. It is worthy of attention that both I_p and P_1 are measurable/computable variables at the transmitter side, which just solves the proposed problem of avoiding bilateral wireless communication.

Firstly, the method for estimating the load output current I_L is derived. When the WPT system operates under resonance and the parasitic resistances R_1 and R_2 are neglected, the RMS value of the emitter current I_p can be determined using Eqns (1), (2), (16), and (18) as:

$$I_{p\_RMS} = \frac{16\sqrt{2} R_L}{\pi^3 (\omega M)^2} U_d \cos\frac{\alpha}{2} \quad (19)$$

From Eqn (19), the variation of R_L affects I_{p_RMS}, and then the adjustment of the current I_L flowing through the battery equivalent load R_L by controlling I_{p_RMS} is analyzed as follows.

$$I_{p\_RMS} = \frac{\pi}{2\sqrt{2}} \frac{I_L}{\omega M} \sqrt{\left(\frac{A}{\omega C_S}\right)^2 + \left(R_2 + \frac{8}{\pi^2} R_L\right)^2} \quad (20)$$

From this it is then possible to deduce the equation for estimating the load output current I_L, where $A = 1 - \omega L_s C_s$.

Secondly extrapolating the estimation method of load resistance, based on Eqn (20) and assuming that the battery is a resistor, it is apparent from Fig. 3 that the impedance Z_1 on the primary side, introduced into the magnetic coupler for S/S compensation, is expressed by the following equation:

$$Z_1 = \left[R_1 + \frac{(\omega M)^2 (\omega C_s)^2 (R_2 + R_o)}{(\omega C_s)^2 (R_2 + R_o)^2 + (1 - \omega^2 L_s C_s)^2}\right] + j\left[\omega L_p + \frac{(\omega M)^2 (\omega C_s)\left(1 - \omega^2 L_s C_s\right)}{(\omega C_s)^2 (R_2 + R_o)^2 + (1 - \omega^2 L_s C_s)^2}\right] \quad (21)$$

Assuming negligible losses on the secondary side, the power delivered to the battery equals power consumption in the actual use of Z_1. The active power P_1 is thus derived as:

$$P_1 = I_{p\_RMS}^2 \left[R_1 + \frac{(\omega M)^2 (\omega C_s)^2 (R_2 + R_o)}{(\omega C_s)^2 (R_2 + R_o)^2 + (1 - \omega^2 L_s C_s)^2}\right] \quad (22)$$

When the system is operating at resonance, the battery equivalent resistance R_L is:

$$R_L = \frac{\pi^2}{8}\left[\frac{(\omega M)^2 I_{P\_RMS}^2}{P_1 - R_1 I_{P\_RMS}^2} - R_2\right] \quad (23)$$

Calculation of resonant frequency

According to Fig. 4, we define $I(\omega)$ as the proportion of output current to input voltage:

$$I(\omega) = \frac{I_o}{U_{in}} = \frac{j\omega M}{Z_1 Z_2 + \omega^2 M^2} \quad (24)$$

According to Fig. 4, we define $E(\omega)$ as the voltage transfer ratio of the output voltage-to-input voltage, which in combination with Eqn (13) yields:

$$E(\omega) = \frac{U_o}{U_{in}} = \frac{j\omega M R_o}{Z_1 Z_2 + \omega^2 M^2} \quad (25)$$

The ω_p and ω_s represent the primary and secondary resonant angular frequencies of the system.

$$\omega_P = \frac{1}{\sqrt{L_P C_P}} \text{ and } \omega_S = \frac{1}{\sqrt{L_S C_S}} \quad (26)$$

In previous applications, their ratios were:

$$\mu = \frac{\omega_P}{\omega_S} \quad (27)$$

We can derive the characteristics of the ideal transconductance $I_i(\omega)$ and the ideal voltage transfer ratio $E_i(\omega)$ by assuming $R_1 = R_2 = 0$. At specific operating frequencies, the transfer functions I_i and E_i exhibit load-independent properties. To identify these specific operating frequencies, we set the R_o coefficients in Eqns (24) and (25) to zero. The load-independent G_i can be operated at ω_p and its magnitude is determined as:

$$|G_i(\omega_P)| = \frac{1}{\omega_P k \sqrt{L_P L_S}} \quad (28)$$

Note that in the design, k is the coupling coefficient, and Eqn (27) should be satisfied that μ is close to 1, i.e., $\omega_p \approx \omega_s$. Similarly, E_i is given by the following equations for a CV output:

$$|E_i(\omega_L)| = \sqrt{\frac{L_S}{L_P}}\left|\frac{k(\mu^2 + 1 - \Delta)}{(2k^2 - 1)\mu^2 + 1 - \Delta}\right| \quad (29)$$

$$|E_i(\omega_H)| = \sqrt{\frac{L_S}{L_P}}\left|\frac{k(\mu^2 + 1 + \Delta)}{(2k^2 - 1)\mu^2 + 1 + \Delta}\right| \quad (30)$$

Included among these, $\Delta = \sqrt{(1-\mu^2)^2 + 4k^2\mu^2}$, the operating angular frequency in CV is given by the following equation:

$$\omega_L = \omega_S \sqrt{\frac{\mu^2 + 1 - \Delta}{2(1-k^2)}} \tag{31}$$

$$\omega_H = \omega_S \sqrt{\frac{\mu^2 + 1 + \Delta}{2(1-k^2)}} \tag{32}$$

Therefore, the WPT system with S/S structure operates at the frequency calculated by Eqn (26) in CC mode and at the frequency calculated by Eqns (31) and (32) in CV mode.

Based on all the theoretical formulas of the WPT system with S/S structure, a set of achievable parameters of the proposed system is designed as presented in Table 1.

Table 1. Theoretical circuit parameters.

Parameters	Value
f_{cc} (kHz)	70
f_{cv} (kHz)	91.7
C_p (nF)	18.546
C_s (nF)	18.221
L_p (μH)	280
L_s (μH)	285
M (μH)	115.918
R_1 (Ω)	0.15
R_2 (Ω)	0.1

Simulation verification of constant current and voltage output of WPT system with S/S topology

Based on the theoretical parameters of Table 1 and simulation of Eqns (6) and (8) by MATLAB, the relationship between the load resistance R_L and the output current and input impedance angle under different frequencies are plotted as illustrated in Fig. 5.

In Fig. 5a, it can be seen that when the frequency is close to 70 kHz, the impedance angle is zero under different loads and implemented ZPA feature. In Fig. 5b, it can be seen that when the frequency is close to 70 kHz, the CC output of 0.38 A can be realized, and although the output current can be higher around 71 kHz, the increase is not large enough to be negligible, and the CC characteristic of the system is weakened at 71 kHz. In summary, the CC resonant frequency of the system is selected as 70 kHz.

The relationship between the load resistance R_L and the output voltage and input impedance angle at different frequencies by simulating Eqns (6) and (12) in MATLAB are shown in Fig. 6.

From Fig. 6a, it can be seen that the S/S topology has a small impedance angle in CV mode and does not achieve the zero phase angle characteristic. From Fig. 6b, it can be concluded that the S/S topology will achieve a CV output of 23 V at a frequency of about 91.7 kHz.

To verify the feasibility of the proposed WPT system with S/S topology, a set of simulation circuits with 0.38 A/23 V charging

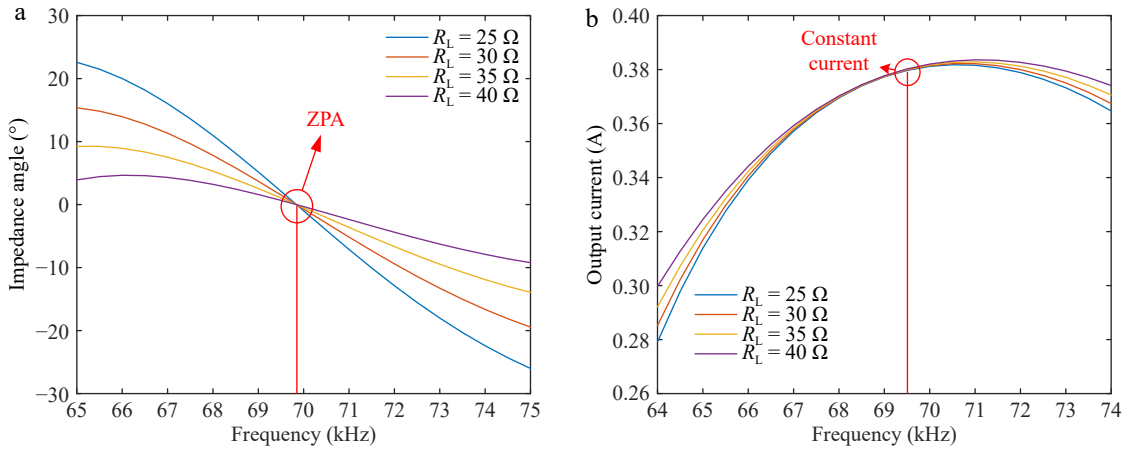

Fig. 5 Relationship between load resistance R_L and output current and input impedance angle under different frequencies in CC mode. (a) Impedance angle under different loads for frequency change. (b) CC output characteristics.

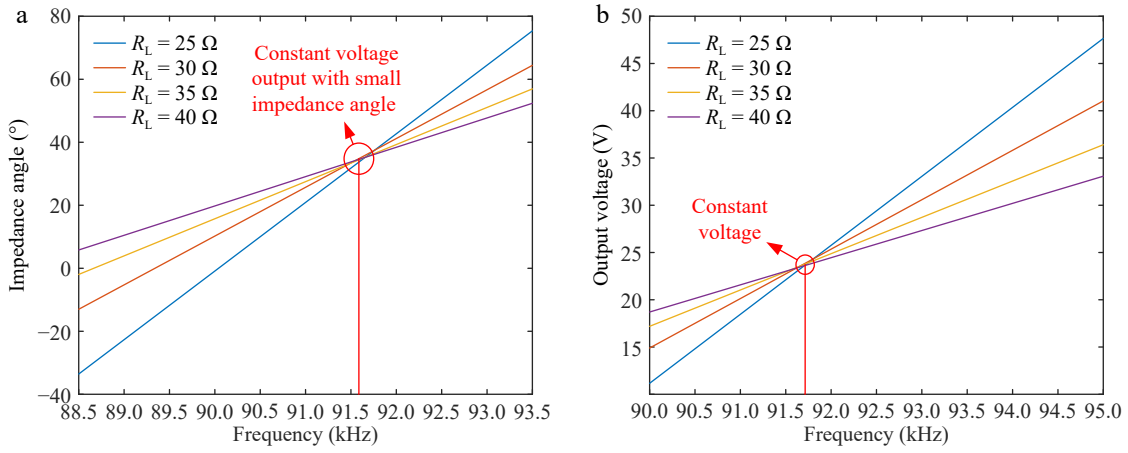

Fig. 6 Relationship between load resistance R_L and output voltage and input impedance angle under different frequencies in CV mode. (a) Impedance angle under different loads for frequency change. (b) CV output characteristics.

output is built in MATLAB/Simulink. The switching strategy of the system is shown in Fig. 7.

The system operates initially at a CC resonant frequency of 70 kHz, delivering a constant current of 0.38 A to the battery load. This phase ensures a stable charging current, as depicted in Fig. 8. During this stage, the charging process starts with a relatively low load resistance, enabling a consistent current supply to the battery. As the charging progresses, the battery's state of charge (SOC) increases, leading to a gradual rise in the load resistance of the system. Consequently, the voltage across the load terminals also increases proportionally, following Ohm's Law. When the charging voltage at the load terminals reaches 23 V, this marks the transition point where the system needs to switch from CC mode to CV mode to ensure safe and efficient charging. At this transition point, the controller on the transmitter side dynamically adjusts the operating frequency of the system from the CC resonant frequency of 70 kHz to the CV resonant frequency of 91.7 kHz. This frequency shift ensures that the system can maintain a stable voltage of 23 V across the load terminals, as illustrated in Fig. 9. During the CV charging phase, the charging voltage remains fixed at 23 V, while the charging current gradually decreases. This decrease is a natural result of the increasing load resistance as the battery approaches full charge. The current continues to decline until it reaches a predefined cutoff threshold, signaling the end of the charging process. This seamless frequency switching between the CC and CV modes, coupled with dynamic voltage and current control, ensures efficient and safe battery charging while protecting the system components from overvoltage or overcurrent conditions.

It is important to note that when the charging voltage reaches the desired value, the resonance frequency is adjusted via the transmitter-side controller without using wireless communication. Instead, the load resistance and charging current are estimated based on known parameters, allowing for an estimation of the charging voltage, which serves as the criterion for frequency switching.

According to Fig. 8, it can be seen that before 0.25 s, the system is able to output a constant charging current of 0.38 A, but as the increase of the load resistance value, the charging voltage increases and when the load resistance value is 62 Ω at 0.25 s, the charging voltage reaches 23 V, then system enters into the CV charging mode.

As illustrated in Fig. 9, when the system is in the transient state at 62 Ω, the charging current is approximately 0.38 A, and the charging voltage is 23 V. After the system transitions to constant-voltage charging, the charging current gradually diminishes with the augmentation of load resistance. Although the charging voltage fluctuates slightly, the fluctuation is negligible and can be approximated as constant-voltage charging.

Since the switching criterion for the resonant frequency in this study is based on whether the estimated charging voltage reaches 23 V, Fig. 10 presents the waveform of the actual charging voltage and the predicted voltage around 0.25 s (when the resonant frequency is switched). It is apparent from Fig. 10 that the actual

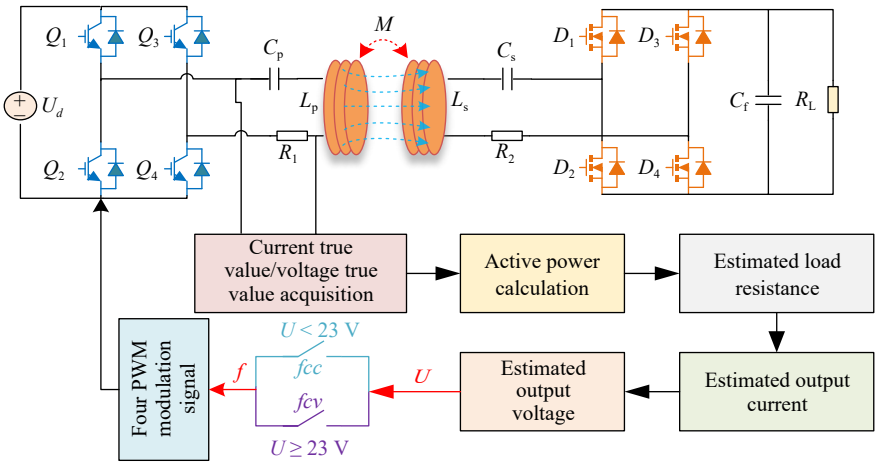

Fig. 7 System switching strategy.

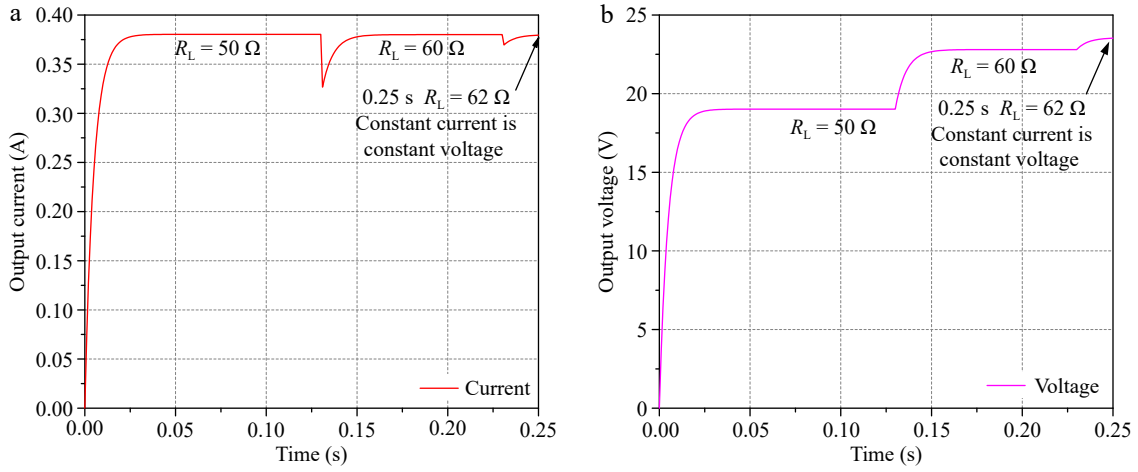

Fig. 8 Current-voltage diagram in constant-current mode. (a) Current. (b) Voltage.

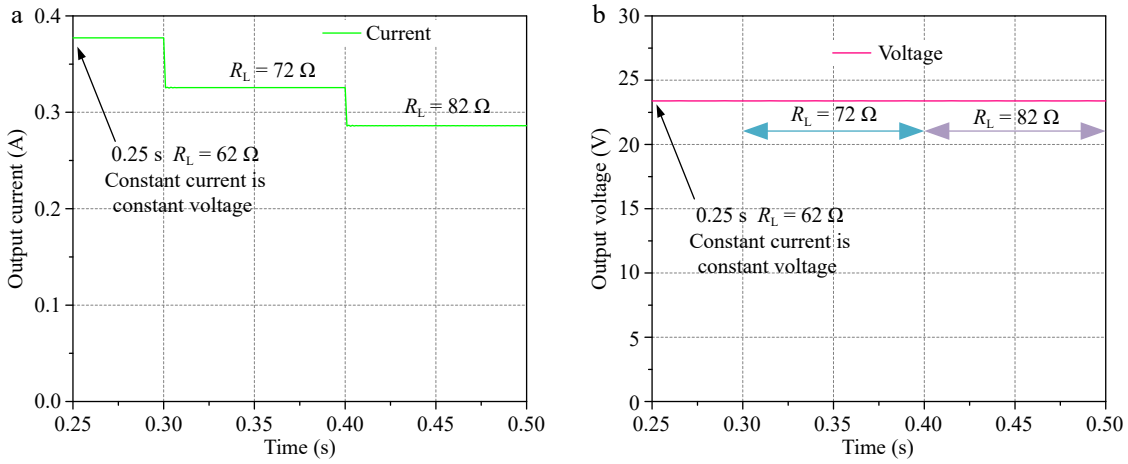

Fig. 9 Current-voltage diagram in constant-voltage mode. (a) Current. (b) Voltage.

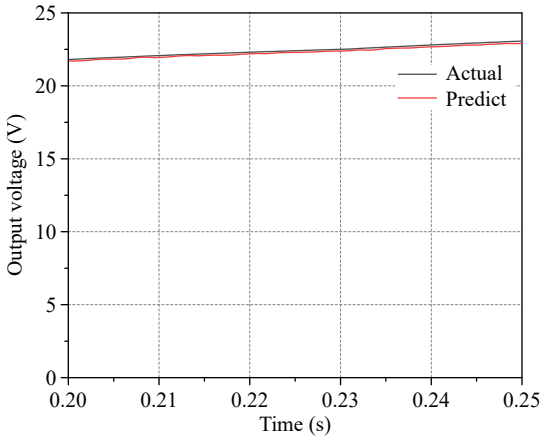

Fig. 10 Predicted and actual voltage waveforms at frequency switching.

charging voltage is in high agreement with the predicted charging voltage, which verifies the rationality of the adopted methodology.

According to Figs 5a and 6a, it can be concluded that in CC mode, when the system running at resonance, the total input impedance Z_{in} is zero, and the current and voltage generated by the inverter's output exhibit Zero Phase Angle (ZPA) characteristics, as illustrated in Fig. 11a. In CV mode, the impedance angle is approximately 30° (with the current lagging the voltage by about 30°) when the system running at resonance, which prevents the realization of ZPA characteristics; however, soft switching can still be achieved, as illustrated in Fig. 11b.

Experimental verification

To verify the above theoretical analysis, the experimental platform shown in Fig. 12, is built on the basis of simulation verification.

Figure 13a shows the experimental waveforms of inverter output voltage U_{in} and inverter output current I_{in} in CC mode, and Fig. 13b shows the current-voltage waveforms in CC mode.

From Fig. 13b, it can be seen that when the load resistance value is 25 Ω, the output current of the system is 0.38 A, with the increase of the load resistance value to 45 Ω, the voltage rises from 10 to 16 V, but the output current is still 0.38 A, and the system realizes the CC output.

Figure 14a shows the experimental waveforms of inverter output voltage U_{in} and inverter output current I_{in} in CV mode, and Fig. 14b shows the current-voltage waveforms in CV mode.

From Fig. 14b, it can be seen that when the load resistance value is 95 Ω, the output voltage of the system is 23 V and the output current is 0.2 A. When the load resistance value is increased to 125 Ω, the output current of the system is reduced to 0.04 A, and the output voltage is still 23 V, which realizes the CV output.

Finally, the efficiency of the system designed in this paper is analyzed, as illustrated in Fig. 15, the efficiency of the system can be obtained and is higher in CC mode due to the ZPA characteristics of the system, which reached 96.5%, and in CV mode due to the presence of small impedance angle, the efficiency of the system reached 95.5%.

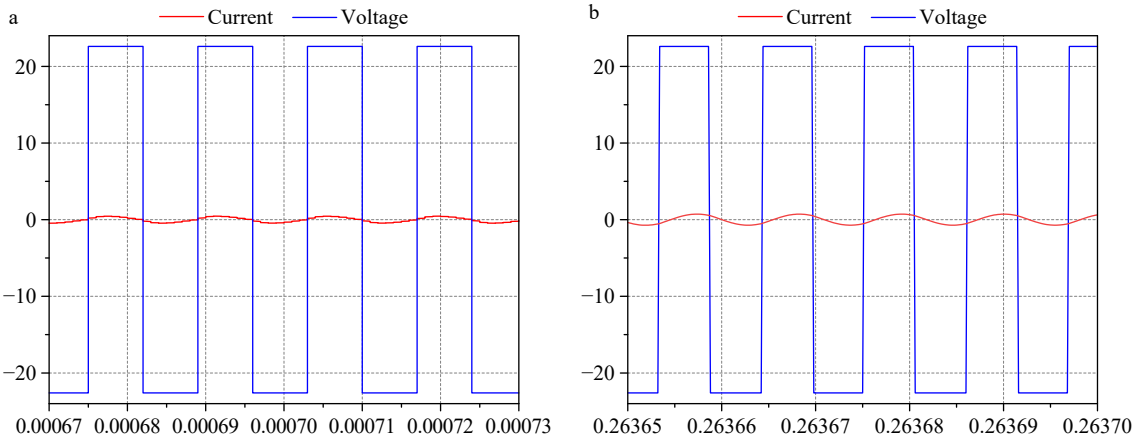

Fig. 11 Voltage-current waveform of inverter output. (a) CC. (b) CV.

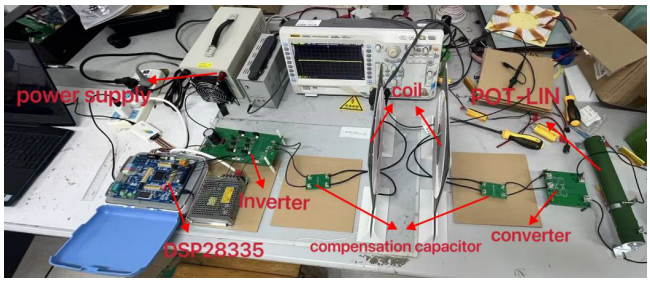

Fig. 12 Experimental platforms.

The efficiency loss of the system is analyzed as shown in Fig. 16, and the efficiency loss is mainly concentrated on the inverter, compensation network, coupler, and rectifier. Since the inverter uses four IGBTs, the operating frequency of the system is not the best operating frequency of IGBTs, so the loss is mainly concentrated in the inverter, but the ZPA characteristics of the system in constant current mode and the ability to realize soft switching in constant voltage mode do not make the system efficiency loss too high; secondly, there is also a loss because the secondary coil can not completely absorb all the power of the primary coil. The rectifier and compensation network also have small losses.

To demonstrate the superiority and innovation of the proposed system design methodology, the WPT technology proposed in this study has undergone a detailed performance comparison with systems documented in existing literature. The detailed comparison results are presented in Table 2. It can be seen that the system designed in this text both uses fewer compensating components and compensates for the shortcomings in the design of other methods.

Discussion

Most of the existing WPT systems rely on wireless communication to realize the switching of operating modes, which puts high requirements on the stability and complexity of the communication system, is susceptible to external interference and may lead to control failure or efficiency degradation, especially under dynamic loads. By switching the resonant frequency without wireless communication and directly utilizing the resonant network characteristics to achieve CC and CV charging, not only the system architecture is simplified and the cost is reduced, but also the robustness of the system is improved. This method can realize more efficient and stable power transmission, which has obvious advantages over traditional methods.

Through this study, the necessity of wireless communication in WPT systems has been reevaluated, providing new design ideas for realizing a more simplified and reliable WPT system. This technique breaks the dependence on traditional communication links and makes WPT applications possible in resource-constrained or high-interference environments.

The study mainly verifies the feasibility of the method of switching resonant frequency, but it has not yet fully explored how to realize the optimal frequency switching strategy under dynamic loading, which can be thoroughly investigated in this direction in the future, and to validate the robustness of the method in more complex scenarios, such as high power and long transmission distance, and to promote its application in real products.

Conclusions

This paper proposes an S/S compensated WPT system to enable battery charging in both constant current and current voltage modes by switching between two specific frequencies. Through circuit structure analysis and theoretical derivation, the system can achieve constant current and current voltage outputs at two fixed resonant frequencies without reconfiguring the circuit structure and without complex closed-loop control. Additionally, an output voltage estimation method is employed, which does not require

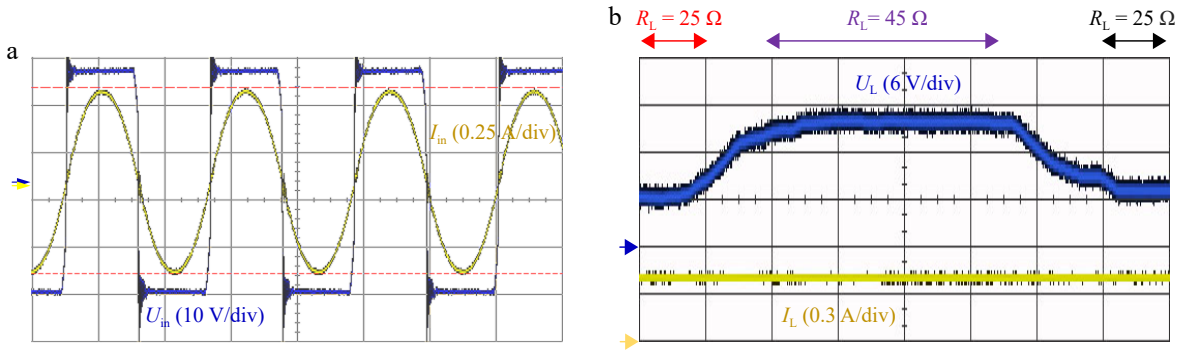

Fig. 13 Experimental diagram of the system in CC mode. (a) Inverter voltage and current phase. (b) Load current and voltage at constant current output.

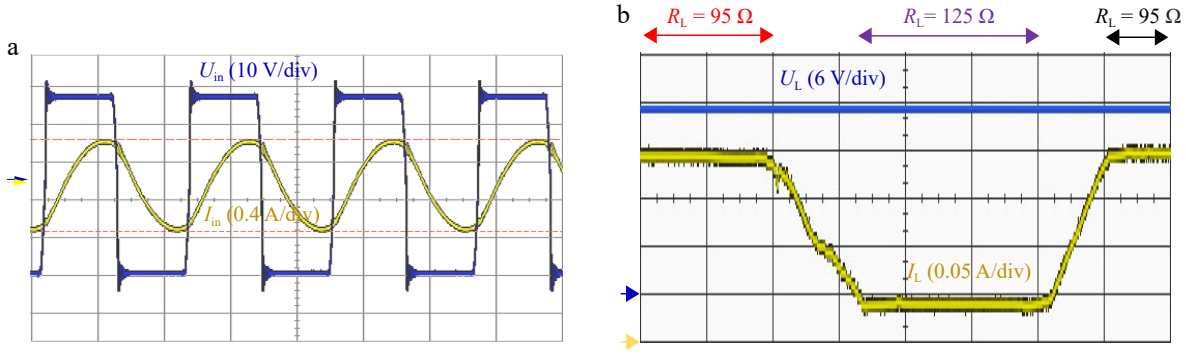

Fig. 14 Experimental diagram of the system in CV mode. (a) Inverter voltage and current phase. (b) Load current and voltage at constant voltage output.

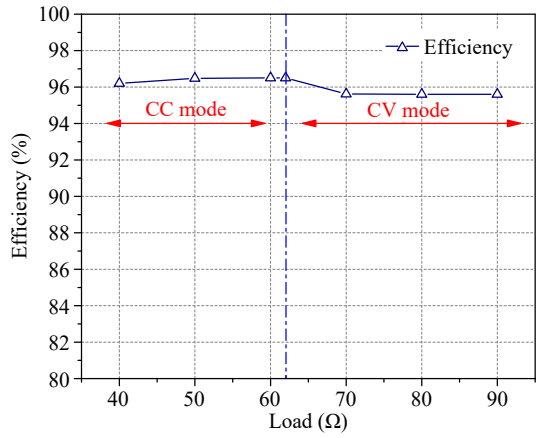

Fig. 15 Efficiency of WPT system with S/S structure.

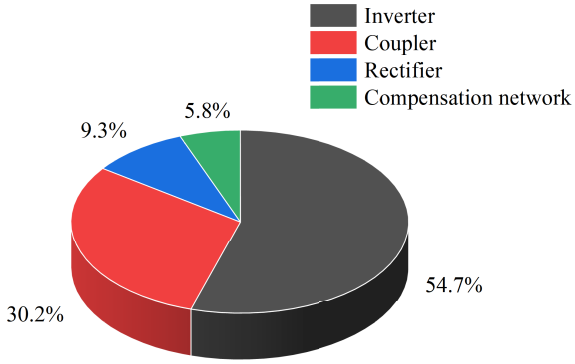

Fig. 16 Analysis of efficiency losses.

Table 2. Comparison of CC and CV output WPT systems.

Compensation elements	Switch topology	DC-DC circuit	Wireless communication	Repeater coil	Ref.
2	×	√	√	×	[9]
6/4	√	×	√	×	[11]
4	×	×	√	×	[12]
4	×	×	√	√	[14]
3	×	×	√	×	[16]
5/7	√	×	√	×	[17]
4	√	×	×	×	[19]
2	×	×	×	×	this paper

√ means used, and × means not used.

wireless communication. Simulation results and experimental results validate that the designed system can achieve a charging output of 0.38 A/23 V, with minimal error between the actual charging output voltage and the estimated output voltage. Finally, the system's efficiency is analyzed, with an efficiency of 96.5% in CC mode and 95.5% in CV mode.

Author contributions

The authors confirm contribution to the paper as follow: study conception and design: Guo Z, Li Z; data acquisition and data collation: Guo Z, Li Z, Yu H, Zhang H; analysis of simulation results: Guo Z, Li Z, Nai J, Chen S; writing manuscript review and editing: Guo Z, Li Z, Liu R; access to funds: Zhang M. All authors have read and agreed to the final version of the manuscript.

Data availability

All data generated or analyzed during this study are included in this published article.

Acknowledgments

This work was supported in part by the Natural Science Foundation of Shangdong Province (Grant No. ZR2022ME214).

Conflict of interest

The authors declare that they have no conflict of interest.

Dates

Received 25 November 2024; Revised 24 February 2025; Accepted 18 March 2025; Published online 9 May 2025

References

1. Zhang Z, Pang H, Georgiadis A, Cecati C. 2019. Wireless power transfer – an overview. *IEEE Transactions on Industrial Electronics* 66(2):1044–58
2. Ramakrishnan V, Savio AD, Balaji C, Rajamanickam N, Kotb H, et al. 2024. A comprehensive review on efficiency enhancement of wireless charging system for the electric vehicles applications. *IEEE Access* 12:46967–94
3. Ma Q, Xu J, Pang S, Li X, Li H, et al. 2024. High efficiency three-dimensional wireless power transfer system using cylindrical transmitting coil. *IET Power Electronics* 17(15):2288–300
4. Li Y, Hu J, Li X, Chen F, Xu Q, et al. 2020. Analysis, design, and experimental verification of a mixed high-order compensations-based WPT system with constant current outputs for driving multistring LEDs. *IEEE Transactions on Industrial Electronics* 67(1):203–13
5. Haerinia M, Shadid R. 2020. Wireless power transfer approaches for medical implants: a review. *Signals* 1(2):209–29
6. Li Z, Li J, Li S, Yu Y, Yi J. 2022. Design and optimization of asymmetric and reverse series coil structure for obtaining Quasi-constant mutual inductance in dynamic wireless charging system for electric vehicles. *IEEE Transactions on Vehicular Technology* 71(3):2560–72
7. Tian X, Liu W, Chau KT, Goetz SM. 2024. Omnidirectional magnetic resonant extender design for underwater wireless charging system. *IEEE Journal of Emerging and Selected Topics in Power Electronics* 12(4):3325–33
8. Mai R, Chen Y, Li Y, Zhang Y, Cao G, et al. 2017. Inductive power transfer for massive electric bicycles charging based on hybrid topology switching with a single inverter. *IEEE Transactions on Power Electronics* 32(8):5897–906
9. Yang TD, Quan DZ, Kang CT, Yu JW. 2017. Design of maximum efficiency tracking control scheme for closed-loop wireless power charging system employing series resonant tank. *IEEE Transactions on Power Electronics* 32(1):471–78
10. Liu N, Habetler TG. 2015. Design of a universal inductive charger for multiple electric vehicle models. *IEEE Transactions on Power Electronics* 30(11):6378–90
11. Yang Y, Jia W, Liang D, Xue J, Li Y. 2023. A self-switching wireless power transfer system based on hybrid topology of LCC-LCC/S with constant current and constant voltage. *Transactions of China Electrotechnical Society* 38(18):4823–4837+4852
12. Zhang L, Li H, Guo Q, Xie S, Yang Y. 2022. Research on constant voltage/current output of LCC-S envelope modulation wireless power transfer system. *Energies* 15(4):1562
13. Rehman M, Nallagownden P, Baharudin Z. 2020. Design of a new hybrid topology of WPT system to achieve load-independent constant-current and constant-voltage output. *Symmetry* 12(9):1453
14. Tran DH, Vu VB, Choi W. 2018. Design of a high-efficiency wireless power transfer system with intermediate coils for the on-board

chargers of electric vehicles. *IEEE Transactions on Power Electronics* 33(1):175–87

15. Yang L, Li X, Liu S, Xu Z, Cai C, et al. 2019. Analysis and design of three-coil structure WPT system with constant output current and voltage for battery charging applications. *IEEE Access* 7:87334–44
16. Lu J, Zhu G, Lin D, Zhang Y, Wang H, et al. 2021. Realizing constant current and constant voltage outputs and input zero phase angle of wireless power transfer systems with minimum component counts. *IEEE Transactions on Intelligent Transportation Systems* 22(1):600–10
17. Gautam KK, Chatterjee A, Santra SB, Prasad D. 2025. Constant Frequency CC-CV Operation of Isolated LLC Resonant DC-DC Converter Using Switched Capacitor Network for WCS. *IEEE Transactions on Power Electronics* 40(1):64–70
18. Lu W, Zhao J, Chen X, Fan Q, Zhang C. 2023. Bilateral control strategy based on LCL-S compensation network wireless charging system without communication. *International Journal of Automotive Technology* 24(1):171–78
19. Vaka R, Keshri RK. 2020. Reconfigurable WPT system for load-independent CC and CV output with transmitting-side control. *IET Electric Power Applications* 14(4):685–94
20. Huang ZC, Wong SC, Tse CK. 2017. Design of a single-stage inductive-power-transfer converter for efficient EV battery charging. *IEEE Transactions on Vehicular Technology* 66(7):5808–21
21. Song K, Li Z, Jiang J, Zhu C. 2018. Constant current/voltage charging operation for series-series and series-parallel compensated wireless power transfer systems employing primary-side controller. *IEEE Transactions on Power Electronics* 33(9):8065–80
22. Li D, Wu X, An C, Gao J, Gao W. 2023. Implementation of ZVS for double-sided LCC inductive coupled wireless power transfer system under constant current/constant voltage operation mode. *IEEE Access* 11:29726–43
23. Wang DS, Deng X, Guan ZM, Liu SL, Yang YQ, et al. 2024. Analysis of output characteristics of wireless power transfer system based on LCC/S-S hybrid compensation structure. *Circuit World* 50(1):172–83